Nuclear Science and Techniques (2026) 37:128
https://doi.org/10.1007/s41365-026-01921-6

Development of a transient neutronics and thermal-hydraulics coupling method for TRIGA reactor

Yi-Qing Zhang[1,2] · Ai-Kou Sun[1,2] · Cheng-Wei Liu[1,2] · Ya-Nan Zhao[1,2] · Tao Yu[1,2] · Qian Guo[2,3] · Zhen-Ping Chen[1,2]

Received: 9 July 2024 / Revised: 10 October 2024 / Accepted: 10 November 2024 / Published online: 17 April 2026

Abstract

The interaction and feedback between 3D neutronics and thermal hydraulics are of great significance in reactor safety analyses, particularly for the TRIGA reactor. Owing to the TRIGA reactor's pulse-transient operation status, the power changes by six to eight orders of magnitude within an extremely short duration; this operation is significantly different from PWRs and imposes some challenges for conventional neutronics methods. To describe the transient status of rod insertion or withdrawal, a novel time-dependent particle transport algorithm based on the combined and moving geometry methods is developed and integrated into the neutronics code MagicMC, which is a Monte Carlo particle transport code developed by the Nuclear Energy and Application Laboratory. Combined with the subchannel model, this work presents neutronics and thermal-hydraulics coupling methods for high-fidelity simulation of the TRIGA reactor. First, a steady-state coupling method is established based on over-relaxation iteration, and the number of neutrons in the Monte Carlo simulation is adaptively controlled according to convergence. Subsequently, a transient coupling method is proposed based on the semi-implicit coupling strategy, and a dynamically changing time-step strategy is designed for the coupling iterative process to achieve reasonable convergence. The parameter mapping strategy between neutronics and thermal hydraulics was constructed using one-to-one mapping and volume weight methods. To verify the reliability of the methods, a JSI TRIGA Mark II reactor was selected as the validation benchmark. The coupling results were in good agreement with the experimental data of the JSI TRIGA Mark II reactor, and the coupling methods achieved a high-fidelity numerical simulation of TRIGA reactor. Therefore, the coupling methods proposed in this paper can provide technical support for reactor experiments and the safe operation of the TRIGA reactor.

Keywords Neutronics · Thermal-hydraulics · Time-dependent Monte Carlo · Transient coupling · TRIGA reactor

1 Introduction

Training Research Isotope General Atomics (TRIGA) is a type of pool-type nuclear research reactor generally used for neutron activation analysis and radiation hardness studies [1–3]. TRIGA has a small core size, strong neutron leakage, and extremely uneven core power and temperature distribution [4]. In addition, owing to the selection of U-ZrH as fuel, it exhibits an extremely high prompt negative temperature coefficient [5], which has led to the development of a special transient operating condition—pulse transient. During the pulse transient, the power changes by six to eight orders of magnitude in a short time (~10 ms) [6]. With such strong core physics field variations, a numerical simulation of the TRIGA reactor is necessary to ensure its reliable operation. High-fidelity transient neutronics

This work was supported by the National Natural Science Foundation of China (Nos. 12475174 and 12542055), the Natural Science Foundation of Hunan Province (Nos. 2022JJ40345 and 2021JJ40445).

✉ Qian Guo
guoqian@usc.edu.cn

✉ Zhen-Ping Chen
chzping@usc.edu.cn

[1] School of Nuclear Science and Technology, University of South China, Hengyang 421001, China

[2] Key Lab of Advanced Nuclear Energy Design and Safety, Ministry of Education, University of South China, Hengyang 421000, China

[3] School of Resource Environment and Safety Engineering, University of South China, Hengyang 421001, China

and thermal-hydraulic coupling provide solutions to this problem.

In general, transient coupling can be divided into explicit, semi-implicit, and implicit coupling according to the different situations of the intercode communication process [7]. This coupling strategy is also applicable to TRIGA reactors. Figure 1 shows the working principles of the different transient couplings. Explicit coupling does not consider convergence in the time step but only data exchange at the beginning of the time step, and the Operator Splitting method [8, 9] is widely used in explicit coupling. Semi-implicit coupling requires iterative calculations at each time step to ensure the calculation accuracy, which is usually based on the Picard iteration method [10–12]. Implicit coupling solves transient problems from the perspective of simultaneous neutronics and thermal-hydraulic equations, with data exchange between the solving steps. Because of this property, achieving full implicit coupling between independent codes of different computational domains is challenging. The JFNK method is typically used for realizing implicit coupling [13, 14]. Because of the temporal behavior of transient coupling, current neutronics solutions in the coupled systems of TRIGA reactors usually use the deterministic method [6, 15, 16], which simplifies the geometry and neutron energy group; thus, obtaining a high-fidelity solution has been challenging in transient coupling.

With advancing computational power, the Monte Carlo (MC) method is increasingly applied in the coupling of transient neutronics and thermal-hydraulics, owing to its precise geometric representation and high-fidelity computational accuracy. Two approaches analyze temporal neutron behavior in MC transient neutron transport methods: the quasi-static method [17, 18] and the time-dependent Monte Carlo (TDMC) method [19, 20]. The quasi-static method solves time-dependent neutron flux as a factorization of the time-independent shape function and time-dependent amplitude function. The amplitude function variation is calculated using the point kinetics model [17], which can suffer from inaccuracy due to discretization [20]. The MC code MagicMC [21], developed by the Nuclear Energy and Application Laboratory (NEAL) at the University of South China, implemented a TDMC particle transport algorithm based on the combing method [22] and moving geometry method. By coupling MagicMC with SubChanFlow, this work presents high-fidelity transient coupling methods for TRIGA reactors, developing an adaptive time-step strategy with semi-implicit transient coupling for TRIGA reactor pulsed transients.

The goal of this study is to establish a high-fidelity neutronics/thermal-hydraulics transient coupling method for TRIGA reactors. First, a novel time-dependent MC particle transport algorithm was established based on the combined and moving geometry methods. The neutronics/thermal-hydraulics coupling method was then developed using MagicMC and SubChanFlow for TRIGA reactors. 1) In Sect. 2, the codes used in the coupling are introduced, the steady-state and transient coupling methods used in this study are proposed, and the convergence of the transient coupling time step is constrained. 2) In Sect. 3, based on the coupling methods, the MC and subchannel code models of JSI TRIGA Mark II reactor are created based on coupling methods, and the relevant geometry and material data of the models are described. 3) Section 4 is the result presentation and experimental comparisons. The experimental data from the JSI TRIGA MARK II reactor were compared and verified using the coupling methods developed in this study. The results show that the coupling method proposed in this study can complete the steady-state and transient simulations of a TRIGA reactor with high accuracy.

2 Neutronics/thermal-hydraulics coupling method based on MagicMC and SubChanFlow

In this study, the MC code MagicMC and subchannel code SubChanFlow (SCF) [23] were used as solvers for neutronics and thermal-hydraulics calculations. The interface for data exchange between codes was built using the C++ language. Serial calculations are performed between the MC and subchannel codes, and the exchange of data fields is a strategy that combines one-to-one grid mapping and the volume weight method [24]. To ensure the computational speed and convergence of the transient calculation, this study adds a time-step optimization module to the transient coupling process and uses semi-implicit coupling to deal with the transient process.

2.1 Neutronics analysis code MagicMC

MagicMC is a neutron/photon transport calculation code based on the MC method, which can complete the modeling of a variety of complex geometries. It has developed a special time-dependent particle transport module for transient neutronics/thermal-hydraulics coupling calculations.

MagicMC coupled with the on-the-fly cross-section generation method can quickly and accurately evaluate the impact of the Doppler effect [25] on the resonance cross sections. Owing to the TRIGA reactor's pulse-transient

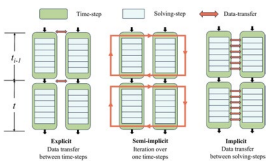

Fig. 1 (Color online) Working principles of explicit, semi-implicit and implicit coupling

operation status, the reactor changes from critical to supercritical and then to subcritical and finally reverts to its critical condition within an extremely short duration. To realize an accurate description of the pulse process induced by the continuous insertion or withdrawal of the pulse rod, MagicMC not only developed a time-dependent geometric movement function (moving geometry method) to describe the rod movement in the reactor, but also calculated the time-dependent power changes under supercritical status through efficient control of the particle population with the combined method. The functional modules of the moving geometry, time-dependent particle transport, on-the-fly cross-section generation, and time-dependent tally developed by MagicMC for neutronic/thermal-hydraulic coupling are shown in Fig. 2.

2.1.1 Moving geometry method

In this study, to realize MC calculations with moving geometries usually occurring under TRIGA reactor transient conditions, MagicMC decomposes the MC model into fixed and moving geometry parts. When the particle enters the moving geometry region, the positions of the moving geometries are recalculated based on the current particle time variable and moving geometry motion parameters (i.e., translation and rotation), and the particle transport calculation is restarted. At the end of the transport time step, the particle time variable and positions of the moving geometries were recalculated, the cell parameters were updated, and the next transport step was started. This cycle is repeated until the particles disappear or leave the moving geometry region. Figure 3 illustrates the particle transport process in a moving geometry.

2.1.2 Time-dependent particle transport with the combing method

In this study, the combination method is introduced as a population control algorithm, which realizes the control of the number of particles by combining the particle weights when the neutron population is increased drastically in the TRIGA pulse-transient operation status. Assuming a total of K particles in the system at moment t, the total weight of the particles accumulated by the system is given by

$$W = \sum_{i=1}^{K} w_i. \tag{1}$$

A data set was generated according to the following method:

$$c_m = \xi \frac{W}{N} + (m-1)\frac{W}{N} \quad m = 1, 2, ..., N \tag{2}$$

where ξ is a uniformly distributed random number from 0 to 1 and N is the number of particles to be maintained.

When c_m falls into the weight interval w_i, the corresponding particle is copied and assigned a new weight value:

$$w_i^{'} = \frac{W}{N}. \tag{3}$$

Figure 4 shows the process of compressing K particles into N particles with weight $w_i^{'}$. Meanwhile, by defining the integer

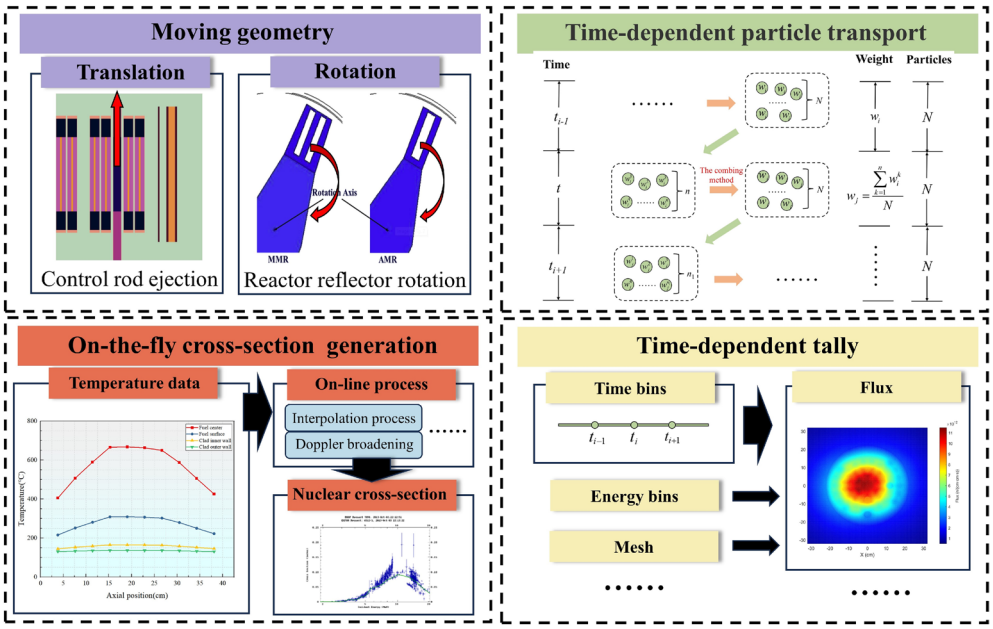

Fig. 2 (Color online) The functions modules developed by MagicMC in response to neutronics/thermal-hydraulics transient coupling

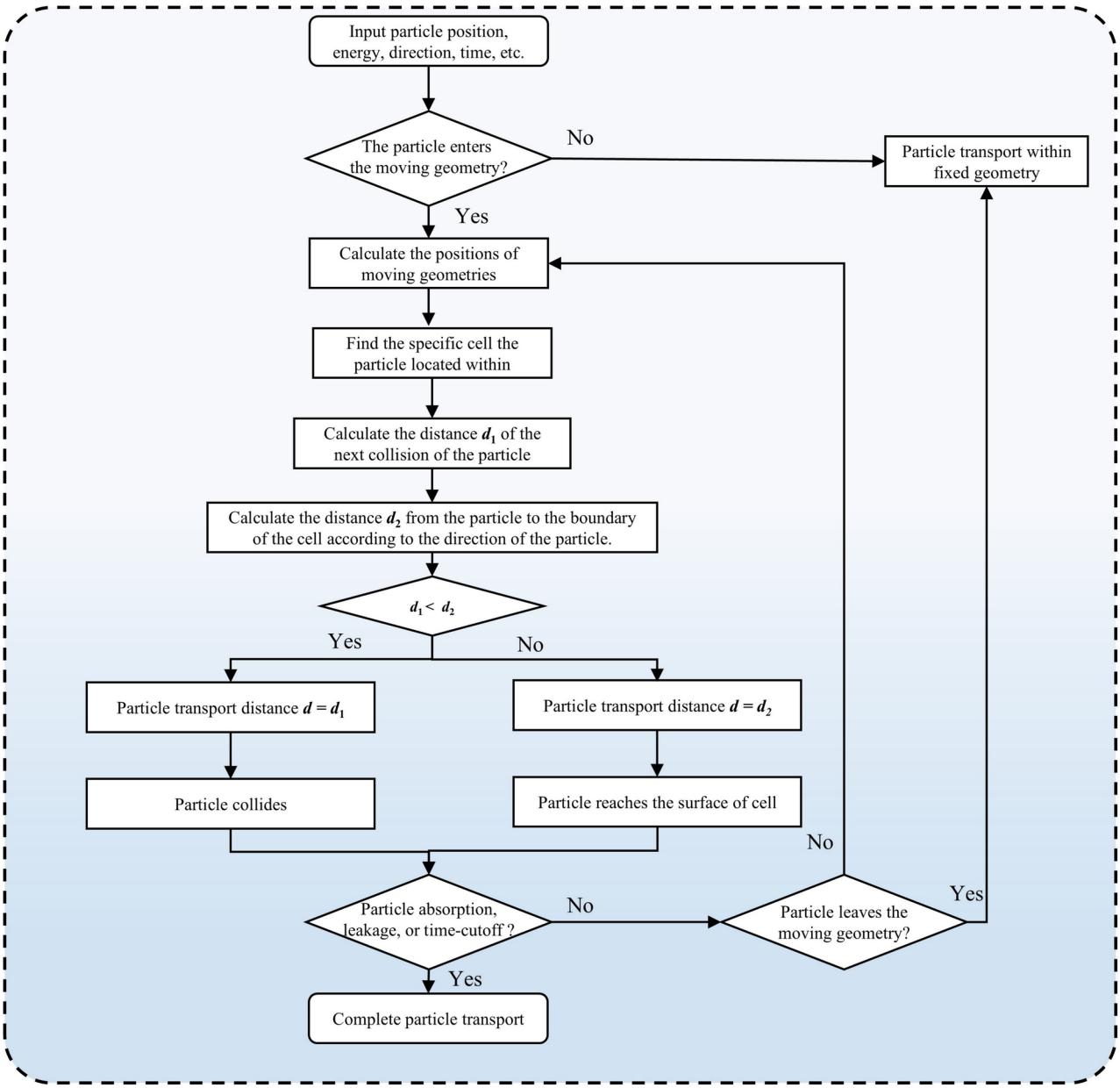

Fig. 3 (Color online) MC particles transport process with moving geometry method

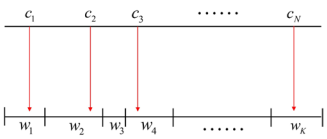

Fig. 4 (Color online) The combing method is used to compressing K particles into N particles

j, particles with weights w_i may produce j particles or $j+1$ particles after combining

$$j < \frac{w_i}{W/N} \leq j+1. \tag{4}$$

The probability of producing j and $j+1$ particles is

$$p_{i,j} = j + 1 - \frac{w_i}{W/N}, \tag{5}$$

$$p_{i,j+1} = \frac{w_i}{W/N} - j. \tag{6}$$

Then, the expected values of the particle weights before and after the compression of the particle with weight $w_i^{'}$ are

$$E[w] = p_{i,j}j\frac{W}{N} + p_{i,j+1}(j+1)\frac{W}{N} = \frac{w_i}{W/N}\cdot\frac{W}{N} = w_i. \quad (7)$$

Therefore, the weights of the particles compressed using the combined method are conserved in the statistics.

2.2 Subchannel analysis code SubChanFlow

SubChanFlow (SCF) is a subchannel-level thermal code for the steady-state and transient analyses of a reactor developed at KIT [26]. This is written entirely in Fortran [27]. Mass conservation, energy conservation, axial momentum conservation, and transverse momentum conservation equations are used to construct the solution model. At present, SCF can define a variety of coolant fluids such as water, lead, lead-bismuth, sodium, etc. Simultaneously, based on the subchannel method, SCF can flexibly divide the control body in the reactor. In theory, SCF can complete the model construction of all rod-fuel reactors. Figure 5 shows the input information and computational flow of SCF.

2.3 Neutronics/thermal-hydraulics coupling method

2.3.1 Steady-state coupling method

Because of the absence of time-dependent treatment methods for the steady-state problem, the steady-state coupling method based on MagicMC and SCF differs significantly from the transient coupling method. The steady-state coupling process uses an overrelaxed iterative method. Steady-state coupling starts with an initial thermal-hydraulic calculation with the power set to a uniform distribution. The calculated temperature and coolant density fields were then passed to the input model of the MagicMC code, and the fuel temperature and coolant density were reset according to the mapping relationship, as shown in Eq. 8. The MagicMC code performs neutron transport to calculate the power distribution and passes it to the SCF model to correct it. Thus, the iterative calculation outputs the results when the convergence conditions are satisfied. The steady-state MagicMC-SCF coupling method is illustrated in Fig. 6. This method uses the infinite norm of the fuel temperature, calculated twice using adjacent iterations, as the convergence condition [28, 29], as shown in Eq. 9.

$$T^n_{\text{fuel}}(i,j,k) = (1-\omega)T^{n-1}_{\text{fuel}}(i,j,k) + \omega T^n_{\text{fuel\_scf}}(i,j,k) \quad (8)$$

$$\in^{L_\infty}_{T_{\text{fuel}}} = \max\left\{\frac{|T^n_{\text{fuel}}(i,j,k) - T^{n-1}_{\text{fuel}}(i,j,k)|}{T^n_{\text{fuel}}(i,j,k)}\right\} \quad (9)$$

where T^n_{fuel} represents the temperature of the reactor fuel, ω is the relaxation factor, ranging from 1 to 2, $T^n_{\text{fuel\_scf}}$ is the calculated fuel temperature for SCF, n indicates the number

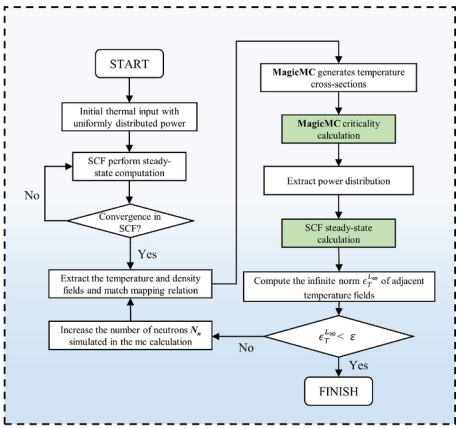

Fig. 6 (Color online) Steady-state coupling method based on MagicMC-SCF

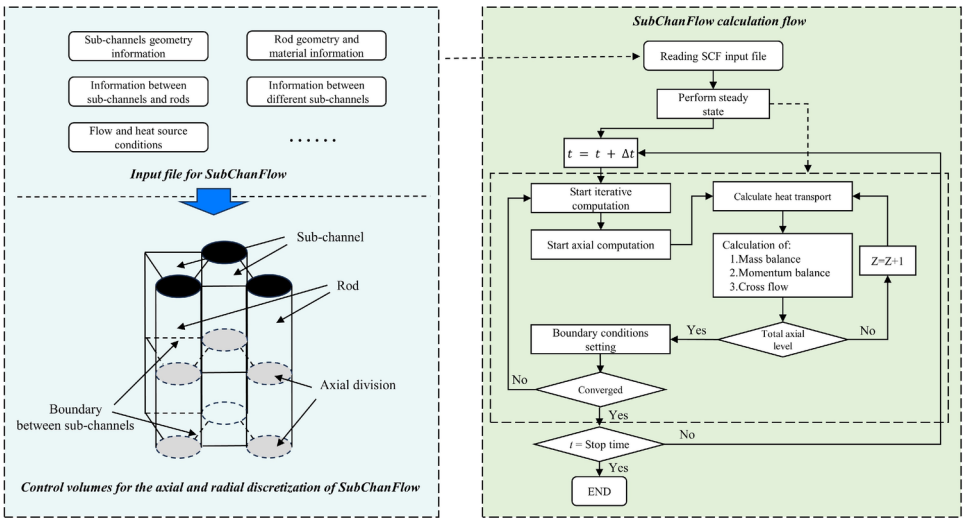

Fig. 5 (Color online) The input information and the computational flow of SCF

of iterations, i, j, k represent the position information of the fuel element, $\in_{T_{\text{fuel}}}^{L_\infty}$ is the relative error calculated at the nth iteration, ε is the convergence criterion. In the MC calculations, the number of simulated particles strongly influenced the convergence of the results. If the number of particles in the calculation is not controlled, it can lead to the method falling into a situation where it cannot converge when the convergence conditions are set too harshly. In addition, considering the error in the initial assumption of uniformly distributed power, an adaptive population control strategy was developed to adjust the number of neutrons in the MC calculations to satisfy the convergence condition in neutronics.

$$N_n = \begin{cases} N_{n-1} & n \le n_{\max} \\ \left[1 + 10(\in_{T_{\text{fuel}}}^{L_\infty} - \varepsilon)\right] N_{n-1} & n > n_{\max} \end{cases} \tag{10}$$

where N_n is the number of particles simulated in the nth iteration of the computational simulation, $n_{\max}$ is the maximum number of iterations used to eliminate errors caused by uniformly distributed power.

2.3.2 Transient coupling method

In the transient analysis, because the time-dependent changes of the neutronics and thermal-hydraulics make the coupling process relatively complex, semi-implicit coupling is used as the time-coupling strategy for MagicMC-SCF coupling in this work. The transient-coupling method is illustrated in Fig. 7.

$$T_{n'}^t(i,j,k) = \begin{cases} T_{n'\_\mathrm{c}}^t & n' = 1 \\ (1-\omega)T_{n'-1}^t + \omega T_{n'\_\mathrm{c}}^t & n' > 1 \end{cases} \tag{11}$$

$$L_\infty^T = \max\{|T_{n'}^t(i,j,k) - T_{n'}^{t-1}(i,j,k)|\} \tag{12}$$

where t is a time point; Δt is the time step; L_∞^T is the infinite norm of the temperature field between adjacent time steps; $T_{n'\_\mathrm{c}}^t$ is the direct result of the coupling method in the n'th iteration of the calculation at the moment t; a is the time step increase factor; b is the time step shortening factor; $N_{\max}$ is the maximum number of iterations, $\Delta T_{\min}$ and $\Delta T_{\max}$ are semi-implicit iterative judgment conditions. As time advances, the code first calculates the infinite norm L_∞^T of the temperature field between adjacent time steps, and determines the convergence of the data in a single time step through semi-implicit coupling. The specific method is as follows.

a) When $L_\infty^T < \Delta T_{\min}$, the data between adjacent time steps are considered to have good convergence and can be output directly. This method carries out transient coupling to advance and lengthen the time step to reduce the number of data exchanges.
b) When $L_\infty^T > \Delta T_{\max}$, the coupling method directly considers that the coupling result has not converged, reduces the time step, and returns to the calculation.
c) When $\Delta T_{\min} < L_\infty^T < \Delta T_{\max}$, the coupling data is considered to be between "convergence" and "non-convergence", and the over-relaxation iteration will be carried out in the time step at this time. During the iteration

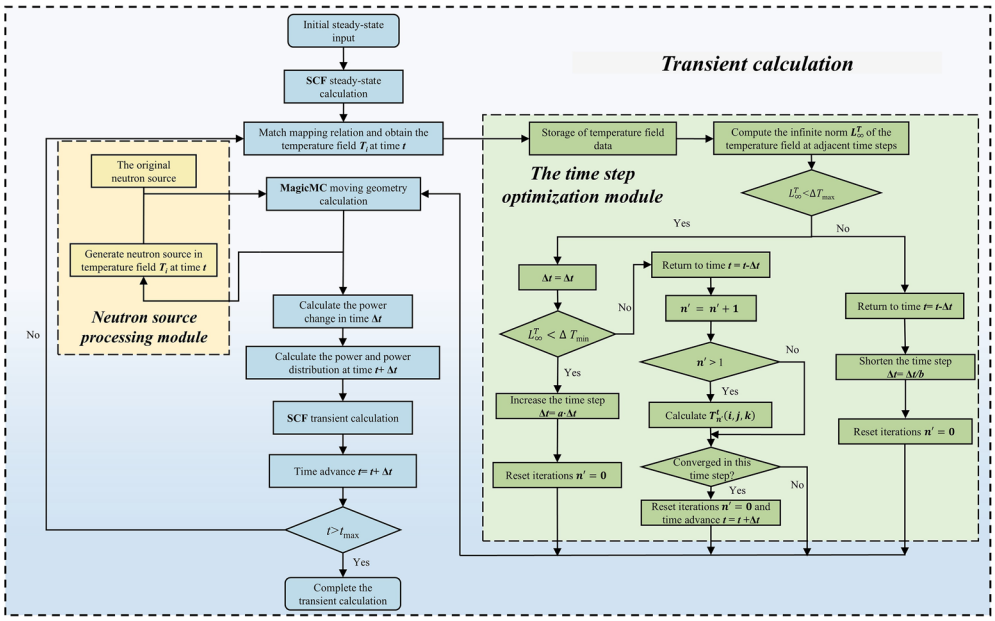

Fig. 7 (Color online) Transient coupling method based on MagicMC-SCF

of this time step, the method still performs computation and judgment of L_{∞}^{T}. If the conditions in (a) or (b) are satisfied, the method prioritizes the execution of the time-step computation strategy in (a) or (b). If the conditions in (a) and (b) are not satisfied, iterations are performed based on the temperatures computed in Eq. 11 until convergence, after which time advancement is performed.

Because the transient coupling calculation is a process advancing with time, in practice, the neutron source calculated at different time steps will theoretically change. The coupling method updates the neutron source in each time step to minimize its influence on the coupling results.

3 Neutronics/thermal-hydraulics models for TRIGA reactor

The TRIGA Mark II research reactor at the JSI is a typical 250 kW TRIGA reactor, which is used for various applications, such as neutron activation analysis, neutron radiography and tomography, education and training, radiation hardness studies, and benchmark experiments for the verification and validation of computer codes [1–3].

Figure 8a–b is the overall design of the JSI TRIGA Mark II reactor [16, 30]. The core of the TRIGA reactor is placed at the bottom of an open tank (atmospheric pressure) with a 5 m water column above it. The core has a cylindrical configuration with 91 designed locations to accommodate fuel elements or other components, such as control rods, a neutron source, and irradiation channels. Figure 8c presents the dimensions of the JSI TRIGA reactor cores. The elements were arranged in six concentric rings: A, B, C, D, E, and F, each with 1, 6, 12, 18, 24, and 30 locations, respectively [31, 32].

3.1 Neutronics model

Two different core arrangements are selected as numerical model for steady and transient states. Core 134 is selected as the steady-state model, and core 231 is selected as the research object for the transient model. The core structure diagram constructed using MagicMC is shown in Fig. 8e. In core 134, all control rods except the regulating rod are fully withdrawn. In core 231, both the safety and shim rods are fully withdrawn, the transient rod (i.e., pulse rod) is fully inserted into the core, and the regulating rod is partially withdrawn to make the core exactly critical.

For the neutronics model, to smooth the temperature and power of the neutronics model, a zirconium rod is designed at the center of the fuel element, and small sections of graphite are designed at the upper and lower ends of the fuel element. The reactor core is reactively controlled by four control rods: a safety rod, shim rod, regulation rod, and transient rod. Except for the transient rod, all the other control rods are designed with a fueled-follower. Figure 8d shows the design scheme of the fueled-follower control rod and fuel element. Cores 134 and 231 are designed with 12 wt% uranium and ^{235}U with 20 % enrichment fuel elements. Table 1 lists the materials and dimensions used in the neutronics model.

3.2 Thermal-hydraulics model

The subchannel division method generally uses the coolant channel as the center [33]. In 2021, Manuel Garcia of KIT analyzed the two partitioning methods centered on the coolant channel and fuel element using the VVER benchmark and concluded that negligible difference existed between the results of the two partitioning methods [29]. Because the TRIGA Mark II reactor uses ring-filled fuel elements for the reactor design, this study adopts a subchannel division method centered on the fuel elements. The core sub-channel division is illustrated in Fig. 8f.

Natural circulation is used to cool the TRIGA reactor. The thermodynamic parameters of fuel U-ZrH are shown in Eqs. 13 and 14 and the thermodynamic parameters of stainless steel are given by Eqs. 15 and 16 [18, 34].

$$C_{v(\mathrm{UZrH})} = 4.17 \times 10^{3} T^{2} + 2.04 \times 10^{6} \tag{13}$$

$$k_{(\mathrm{UZrH})} = 0.0075T + 17.58 \tag{14}$$

$$C_{v(\mathrm{S.S})} = 2.88 \times 10^{3} T^{2} - 9.645 \times 10^{5} T + 1.037 \times 10^{8} \tag{15}$$

$$k_{(\mathrm{S.S})} = -3.3 \times 10^{-6} T^{2} + 1.70 \times 10^{-2} T + 14.280 \tag{16}$$

where C_v is the heat capacity per unit volume, J/(m^3·K)is the unit, and k is the thermal conductivity in units of W/(m·K).

3.3 Spatial mapping method

Spatial mapping methods can be divided into volume weighting and one-to-one mapping methods. Because no power is released from the coolant during the actual calculation, the data processing for the fuel element and coolant differ. The main data used for the mapping are power, temperature, and density. The following method is used to map the data:

a) In the mapping of the power data, the calculation is completed using the MagicMC code, ignoring the release of power in the coolant, only mapping the power data of the fuel element, and the mapping mode is one-to-one map-

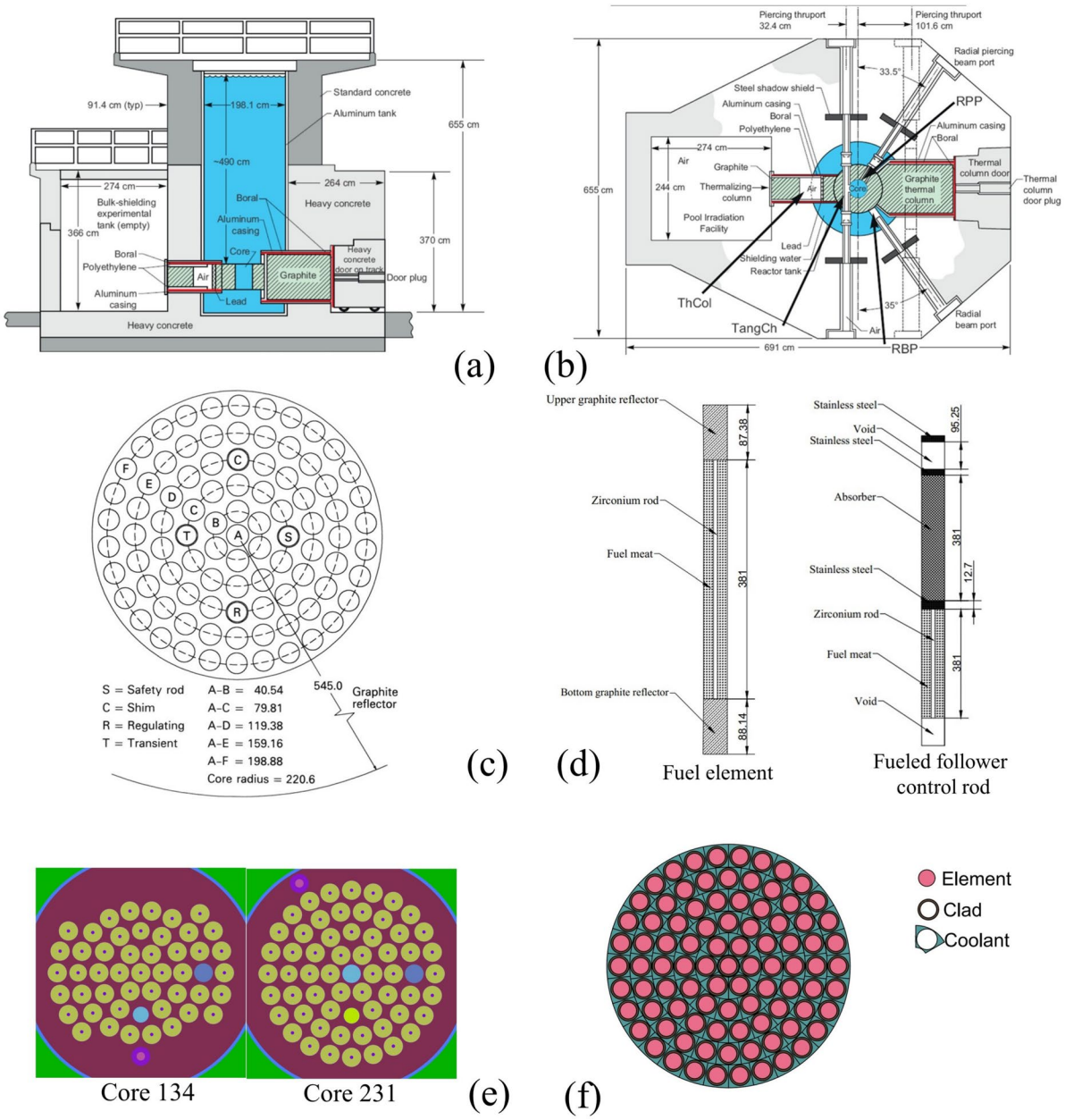

Fig. 8 (Color online) Neutronics/thermal-hydraulics models for TRIGA reactor **a** Side view of the JSI TRIGA Mark II reactor [16, 30]. **b** Top view of the JSI TRIGA Mark II reactor [16, 30]. **c** Top view and ring division of JSI TRIGA reactor core (mm) [31]. **d** Fueled-follower control rod and fuel element (mm). **e** Top view of MagicMC models of core134 and core 231. **f** JSI TRIGA Mark II reactor core sub-channel division

ping. This simplification is verified in the power density calculation of steady-state coupling.

b) In the mapping of the temperature data, we divided the temperature data into the temperature of the rod bundle and that of the coolant. For the rod bundle, a one-to-one mapping method is used to map the temperatures of the fuel, control rod, cladding, and other structures. Figure 9 shows ring B as an example of a radial temperature-mapping scheme, which is divided into 10 nodes in the axial direction for data mapping.

c) For the coolant density, the volume weight method is used to map the data and calculate the average density according to the position of the coolant ring. In the mapping of the reactor material density, the changes in the density of the fuel and cladding structure are ignored,

Table 1 JSI TRIGA Mark II reactor geometry and material information [31]

Component		Dimension (cm)	Material
Reflector	Thickness	13.6500	Graphite
	Height	56.6000	Graphite
	Casing	0.6000	Aluminum
Fuel element	Outside diameter	3.7600	–
	Element length	72.0600	–
	Fuel meat diameter	3.6500	U-ZrH[1]
	Thickness of cladding	0.0508	Type 304 stainless steel
	Diameter of central hole	0.6350	Zirconium
	Fuel meat height	38.1000	–
	Axial bottom reflector	8.8140	Graphite
	Axial top reflector	8.7380	Graphite
Fueled-follower control rod	Total length	111.1250	–
	Fuel meat length	38.1000	U-ZrH
	Absorber length	38.1000	B_4C
	Outside diameter	3.4925	–
	Thickness of cladding	0.0508	Type 304 stainless steel
	Fuel meat diameter	3.3299	U-ZrH
	Absorber diameter	3.3299	B_4C
	Diameter of central hole	0.6350	Zirconium
Transient rod	Outside diameter	3.1750	–
	Clad thickness	0.0711	Aluminum
	Absorber length	38.1000	B_4C
	Air follower length	38.1000	Void
Neutron source	Outside diameter	3.7600	Void + Ra-Be
	Thickness of cladding	0.0508	Aluminum

[1]The 12 wt% uranium and ^{235}U of 20 % enrichment fuel meat, and hydrogen-zirconium atom ratio is 1.65

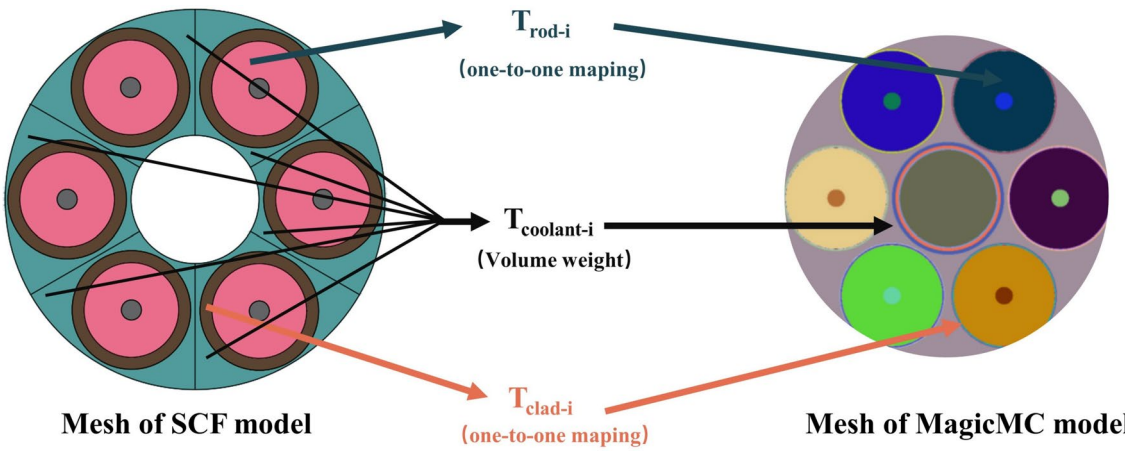

Fig. 9 (Color online) Spatial mapping of temperature data (10 nodes in axial direction)

and the density does not change during the coupling calculation process.

4 Experimental and numerical results comparisons

4.1 Steady-state coupling results

The steady-state calculation used core 134 as the research analysis model, and two different power levels, 125 kW and 250 kW, were calculated. The two power levels were regulated by the position of the regulating rod, and the remaining control rods were fully withdrawn. At 125 kW and 250 kW, the regulating rod was inserted up to 19.4 cm and 13.7 cm, respectively; the coolant inlet temperature was 21.6 °C at both the power levels. Table 2 lists the information on k_{eff} for the steady-state coupling of the two power levels.

Figure 10a–b shows the pin-wise distribution of radial power factor. The standard deviation of all power factors did not exceed 0.003. It can be observed that the power factor of ring B is higher than that of ring A for both power levels, and this result follows the value of the fuel elements of rings A and B in [31]. Because the steady-state power is controlled using only the insertion behavior of the rod R, the power factors of the rod R and its nearby elements differ significantly at the two power levels. In addition, the pin-wise power peak factors at 125 kW and 250 kW are 1.3734 and 1.3403, respectively, which verifies that the deeper the R-rod is inserted, the more uneven the core power distribution. To demonstrate high-fidelity power distribution, Fig. 11a–b shows a finer radial power density distribution in the active zone of the core at 125 kW and 250 kW using an x–y grid of 500×500.

The normalized power distribution is calculated in the axial direction of the reactor and the results are shown in Fig. 11c. The relative axial position of only the active zone of the core is calculated, with the bottom corresponding to the relative position 0 and the top corresponding to the relative position 1. The axial power peaking factors at 125 kW and 250 kW are 1.288687 and 1.300017, respectively.

Figure 11d shows a comparison of the calculated and experimental values of the fuel temperature for different rings. Table 3 compares the calculated and experimental temperatures at certain fuel locations. These temperatures are located ~7 mm from the center of the fuel element in the radial direction and their axial position is at half the height of the fuel meat. The accuracy of absolute temperature measurements in the experiments, due to calibrating uncertainty, is estimated ±3 °C [31]. The temperatures calculated in this study are consistent with the experimental values. The main error arises from the necessary model simplification required for the code-based computation.

Table 2 k_{eff} for steady-state coupling of two power levels

Power (MW)	R control rod insertion (cm)	k_{eff}	Standard deviation of k_{eff}
125	19.4	1.00007	0.00022
250	14.4	1.00026	0.00020

4.2 Pulse transient coupling results

The transient calculations use core 231 as the analysis model. During the transient calculation, the safety and shim rods are fully withdrawn, and reactivity is introduced by withdrawing the transient rod for a short time (~ 80 ms). The integral value of the transient rod under core 231 is calculated to select the correct position for the transient rod. The reactivity worth of the transient rod is calculated using the positive-period method [35], as shown in Eq. 17 and the error propagated during the calculation is given by Eq. 18 [36].

$$\rho = \left(1 - \frac{1}{k_{\text{eff}_0}}\right) - \left(1 - \frac{1}{k_{\text{eff}}}\right) = \frac{1}{k_{\text{eff}}} - \frac{1}{k_{\text{eff}_0}} \tag{17}$$

$$\Delta\rho = \left[\left(\frac{\Delta k_{\text{eff}}}{k_{\text{eff}}}\right)^2 + \left(\frac{\Delta k_{\text{eff}_0}}{k_{\text{eff}_0}}\right)^2\right]^{1/2} \tag{18}$$

where k_{eff_0} denotes the effective multiplication factor. Subsequently, one of the control rods is withdrawn at a certain position by calculating a new k_{eff}. Δk_{eff_0} and Δk_{eff_0} are the fractional statistical error estimates for k_{eff_0} and k_{eff}, respectively.

The integral worth of the transient rod in core 231 is shown in Fig. 12a. Compared to the reactivity value of the transient rod measured in the experiment [6], the integral value of the transient rod is roughly consistent with the experimental value, and the main error arises from the uncertainty of the model simplification construction and nuclear data.

Based on the calculated integral worth of the core 231 transient rod, this study used a coupled code to perform a reactivity insertion pulse transient simulation. The reactor started with an initial power of 100 W and coolant temperature of 21.6 °C. The length required for the transient rod to be withdrawn was calculated based on the integral value of the transient rod, as shown in Fig. 12a. The fixed-source mode was used to calculate the power change in the reactor in a single time step. The shortest timescale of the power change in a single step was 0.002 ms (the minimum scale of the solving step).

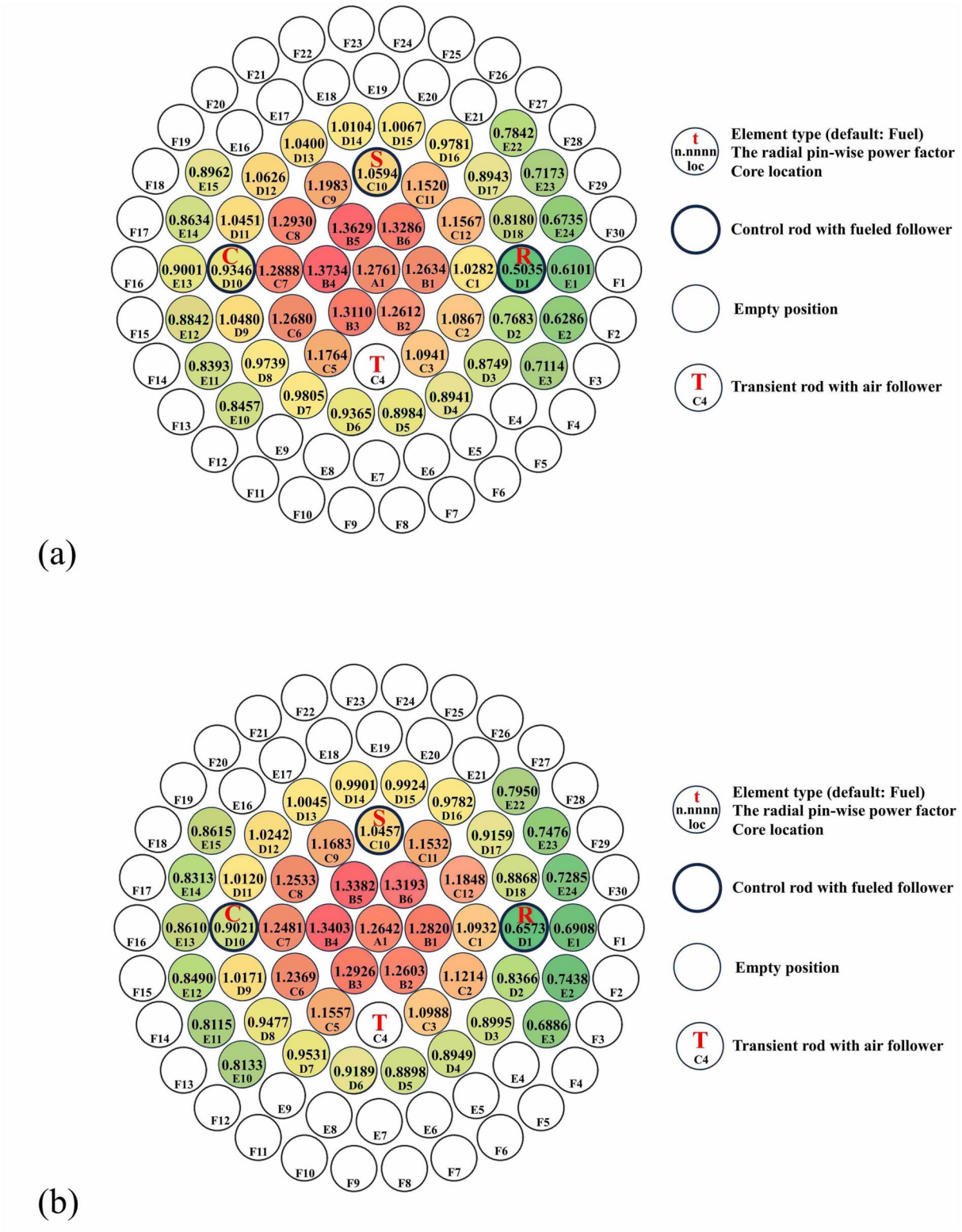

Fig. 10 (Color online) Radial pin-wise power factor distribution (R is regulating rod, C is shim rod, S is safety rod, and T is transient rod). **a** Pin-wise power factor distribution at 125 kW. **b** Pin-wise power factor distribution at 250 kW

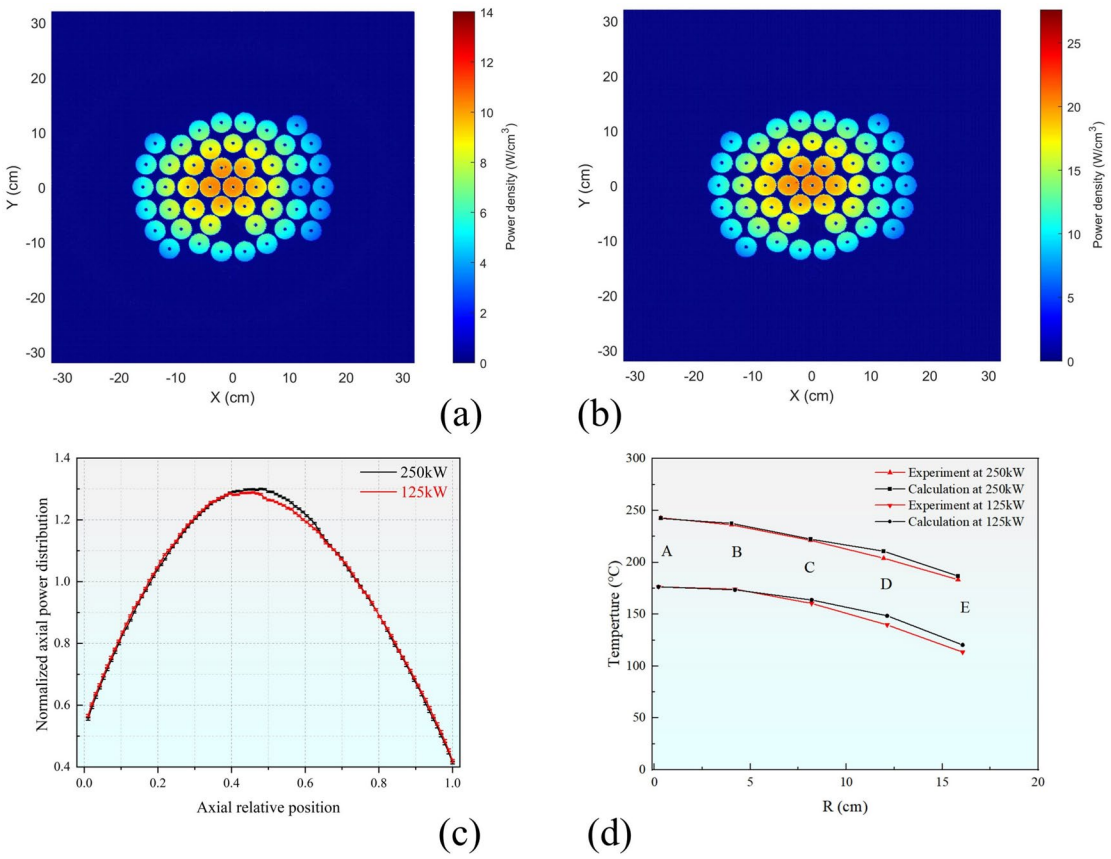

Fig. 11 (Color online) Steady-state coupling results. **a** Radial power density distribution at 125 kW. **b** Radial power density distribution at 250 kW. **c** Normalized axial power distribution **d** Fuel temperature in different rings at 125 kW and 250 kW

Table 3 Temperature comparison between coupling calculation and experiment for the steady-state condition

Location[a]	Fuel temperature (°C)			
	$P = 250$ kW		$P = 125$ kW	
	Calculation	Experiment	Calculation	Experiment
A-1	242.57	244.00	176.37	176.00
B-2	237.65	240.00	173.55	171.00
C-8	223.82	225.00	167.22	164.00
C-9	217.98	218.00	159.46	–
D-11	210.62	211.00	148.47	139.00
D-13	210.74	201.00	148.50	–
E-14	186.73	184.00	120.40	115.00

[a]Information about the location can be found in Fig. 10

The pulse power as a function of time is shown in Fig. 12c–d. To analyze the error source, the peak power of the power curve, calculated using the coupling code, was aligned with the experimental value. Table 4 compares the calculated and experimental values of the key parameters of the pulse-coupling model. The experimental data used in this study were obtained from the JSI public TRIGA pulse experiment, which can be found on the webpage http://trigapulse.ijs.si/. By comparing the power curve and pulse parameters, the coupling method proposed in this work was found to accurately simulate the pulse transient of the TRIGA reactor. The calculated and experimental power change curves are generally consistent. Small differences exist only in regions where the power varies relatively slowly because the presence of delayed neutrons in these regions affects the power variations. In the two simulations, the relative errors between the calculated and experimental values of the peak power were 0.705% and 1.834%, respectively, and the relative error of the maximum fuel temperature did not exceed 4.5%.

Figure 13a–b displays the temperature distribution at different time steps under two transient coupling calculations. The temperature decreased from the inside to the outside. However, the positions of the center and transient control rod do not have a fission power release; therefore, heat cannot be transferred to these locations in a short pulse time. Consequently, their temperatures were significantly lower than those of other parts of the core.

Because the coupling code uses MC for 3D neutronics calculations, it can output neutron flux distributions for

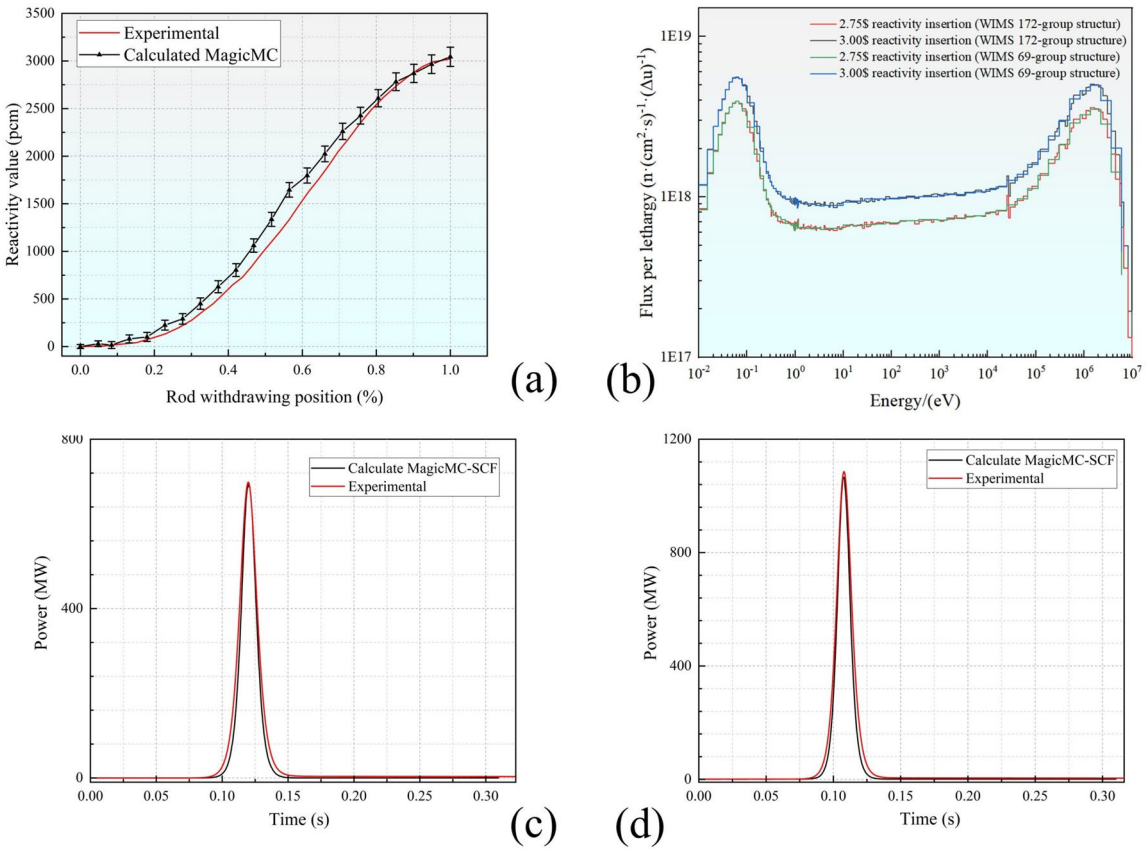

Fig. 12 (Color online) Pulse transient coupling results **a** Comparison of MagicMC and experimental transient rod integral worth in core 231. **b** Neutron energy group distribution at the central guide tube at peak power for two transient conditions. **c** Variation of power over time in 2.75$ reactivity insertion **d** Variation of power over time in 3$ reactivity insertion

different energy groups at different time steps. The central guide tube was selected as the analysis model, and the WIMS 69-group and WIMS 172-group structure [37] were used as the energy group division method. The flux distribution per lethargy of groups 69 and 172 at the central guide tube when the peak power was reached under the two transient conditions is shown in Fig. 12b. The fluxes per lethargy for the different energy-group structures were in good agreement. Because the two-pulse calculations had little effect on the core structure, the relative flux distributions under different energy groups were basically the same. A distinct difference is observed only in the flux magnitude per lethargy mainly because of the difference in the peak power owing to the magnitude of the reactivity insertion.

4.3 Computing environment

All calculations were performed on a computer with an Intel Core i5-13600KF CPU and 48 GB RAM. The calculations were performed using Linux with the CPU operating at a stable frequency of 4.6 GHz. An OpenMP parallel programming model with 20 threads was used for the computations.

In the steady-state coupling, the calculations were performed with 100 inactive cycles followed by 1000 active cycles, with 5000 neutrons per generation. The convergence condition ($\in^{L_\infty}_{T_{\text{fuel}}}$) for the coupled system is set to 0.002. For 125 kW operation, the coupled system converges after 59 iterations, and the number of neutrons computed per generation increases to 22533. For 250 kW operation, the convergence condition is reached after 49 iterations, and the number of neutrons computed per generation increases to 26629. The runtime for both the calculations was approximately 3 h.

In transient coupling, MagicMC used 1.5 million particles in each time bin, and the time bins under a single coupling time step were evenly divided into 100. In the adaptive time-step strategy, we set $\Delta T_{\max}$ and $\Delta T_{\min}$ to 6 °C and 2 °C, respectively, which controlled the time-step behavior of the coupled system. Semi-implicit calculations at a single time step were considered to converge when L^T_∞ was less than 2 °C. The calculated runtime was approximately 28 h with 2.75$ reactive insertion and approximately 30 h with 3$

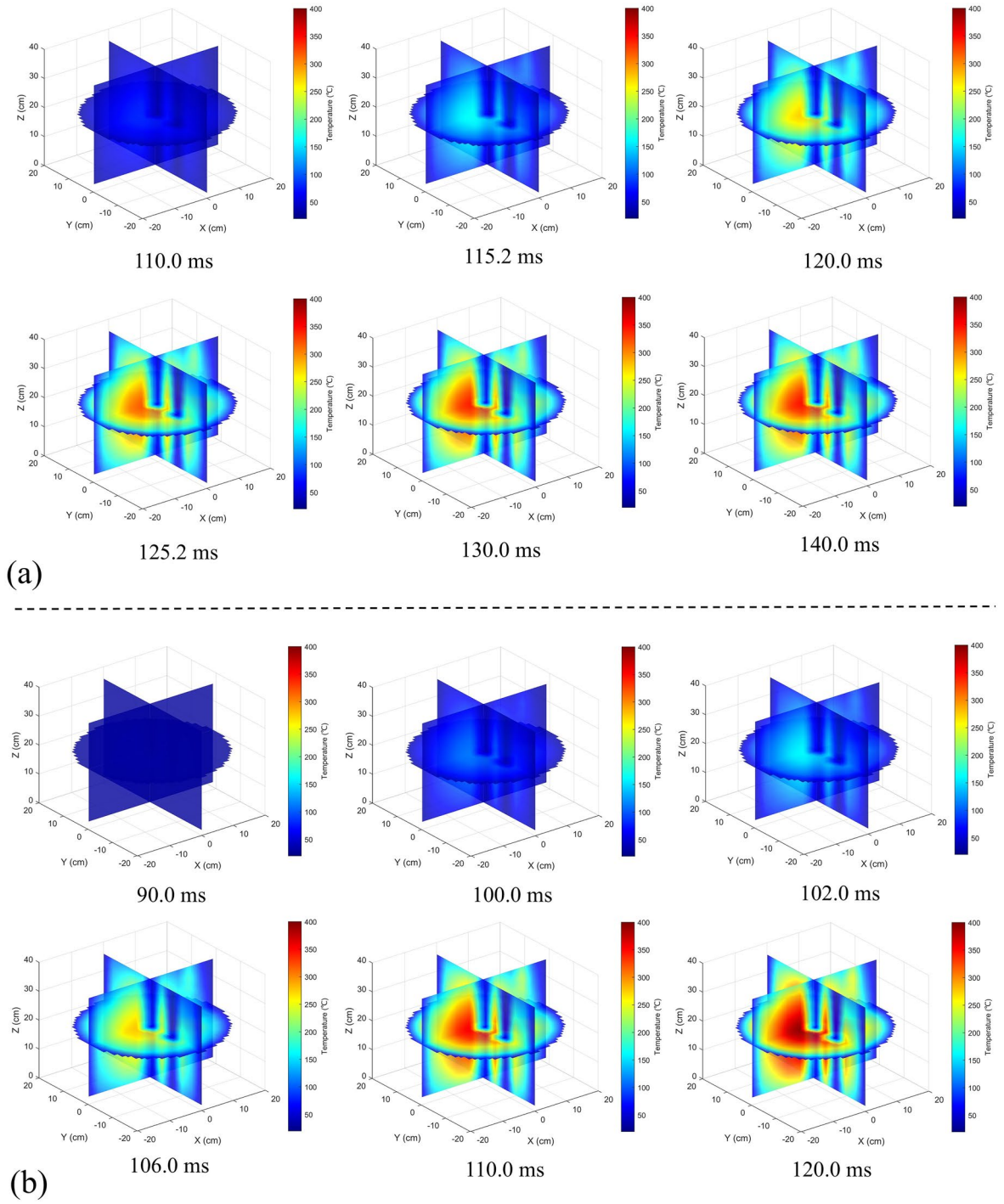

Fig. 13 (Color online) **a** Element temperature distribution at different time step in 2.75$ reactivity insertion. **b** Element temperature distribution at different time step in 3$ reactivity insertion

Table 4 Comparisons between coupling calculation and experiment for the pulse transient conditions

No.	Data source	ρ (\$)	P_{max} (MW)	T_{max} (°C)
1	Calculation	2.789	693.573	360.06
	Experiment	2.750	698.500	373.00
2	Calculation	3.052	977.054	398.81
	Experiment	3.000	995.300	406.10

reactive insertion, and the minimum time step for coupling was 0.0004s.

5 Conclusion

To describe the typical transient conditions of the TRIGA reactor in detail, neutronics/thermal-hydraulics coupling method based on MC and subchannel methods was used in this study. Functional modules of the moving geometry and time-dependent particle transport were developed using MagicMC to satisfy the 3D transient neutronics simulation of the TRIGA reactor. Two coupling methods are proposed for the steady-state and pulse transient conditions of the TRIGA reactor: 1) The steady-state coupling method is based on the over-relaxation iterative method, and the temperature field is chosen as the convergence condition of the coupling calculation to successively approach the steady-state solution. 2) The transient coupling method uses semi-implicit coupling to control the length of the time step and iteration process using convergence evaluation criteria. Simultaneously, the source distribution is adaptively updated using MC iterations to ensure an accurate description of the source term. Based on the above coupling methods, the JSI TRIGA Mark II reactor was selected as the analytical model for validation. The numerical results show that the steady-state and transient neutronics/thermal-hydraulics coupling method proposed in this study can successfully realize the coupling simulation of the corresponding operating conditions, which can provide technical support for reactor experiments and safe operation of the TRIGA reactor.

Author contributions All authors contributed to the study conception and design. Code development, model construction, data processing, code usage guidance, theoretical guidance, manuscript revision, and code support performed by Yi-Qing Zhang, Ai-Kou Sun, Cheng-Wei Liu, Ya-Nan Zhao, Tao Yu, Qian Guo, Zhen-Ping Chen. The first draft of the manuscript was written by Yi-Qing Zhang and all authors commented on previous versions of the manuscript. All authors read and approved the final manuscript.

Data availability The data that support the findings of this study are openly available in Science Data Bank at https://cstr.cn/31253.11.sciencedb.35435 and https://doi.org/10.57760/sciencedb.35435.

Declarations

Conflict of interest The authors declare that they have no conflict of interest.

References

1. V. Radulovic, Ž. Stancar, L. Snoj et al., Validation of absolute axial neutron flux distribution calculations with MCNP with ^{197}Au (n, γ) ^{198}Au reaction rate distribution measurements at the JSI TRIGA Mark II reactor. App. Radiat. Isotopes. **84**, 57–65 (2014). https://doi.org/10.1016/j.apradiso.2013.11.027
2. A. Stergarsek, M. Horvat, P. Frkal et al., Removal of Hg^0 in wet FGD by catalytic oxidation with air–a contribution to the development of a process chemical model. Fuel **107**, 183–191 (2013). https://doi.org/10.1016/j.fuel.2012.08.001
3. A. Kolsek, V. Radulovic, A. Trkov et al., Using TRIGA Mark II research reactor for irradiation with thermal neutrons. Nucl. Eng. Des. **283**, 155–161 (2015). https://doi.org/10.1016/j.nucengdes.2014.03.012
4. R. Li, L. Wang, J. Liang et al., MC/sub-channel coupling for steady state and transient simulation of Xi'an Pulsed Reactor. Ann. Nucl. Energ. **210**, 110882 (2025). https://doi.org/10.1016/j.anucene.2024.110882
5. W. Tan, P. Long, G. Sun et al., Neutronics analysis of JSI TRIGA Mark II reactor benchmark experiments with SuperMC33. Nucl. Eng. Technol. **51**(7), 1715–1720 (2019). https://doi.org/10.1016/j.net.2019.05.014
6. I. Švajger, D. Čalic, A. Pungercic et al., Evaluation of reactor pulse experiments. Nucl. Eng. Technol. **56**(4), 1165–1203 (2024). https://doi.org/10.1016/j.net.2023.11.021
7. K. Zhang, Multi-scale thermal-hydraulic developments for the detailed analysis of the flow conditions within the reactor pressure vessel of pressurized water reactors, Dissertation. Karlsruhe Inst. Technol. (2020). https://doi.org/10.5445/IR/1000105872
8. C. Zhao, Z. Liu, L. Liang et al., Improved leakage splitting method for the 2D/1D transport calculation. Prog. Nucl. Energ. **105**, 202–210 (2018). https://doi.org/10.1016/j.pnucene.2018.01.007
9. R.I. McLachlan, G.R. Quispel, Splitting methods. Acta. Numer. **11**, 341–434 (2002). https://doi.org/10.1017/S0962492902000053
10. J.C. Almachi, V. Sánchez-Espinoza, U. Imke et al., Validation of the dynamic simulation capabilities of Serpent2/Subchanflow using experimental data from the research reactor SPERT IV D-12/25. Nucl. Eng. Des. **418**, 745–762 (2024). https://doi.org/10.1016/j.nucengdes.2023.112840
11. A.G. Mylonakis, M. Varvayanni, N. Catsaros et al., Multi-physics and multi-scale methods used in nuclear reactor analysis. Ann. Nucl. Energ. **72**, 104–119 (2014). https://doi.org/10.1016/j.anucene.2014.05.002
12. H. Zhang, J. Guo, F. Li et al., Efficient simultaneous solution of multi-physics multi-scale nonlinear coupled system in HTR reactor based on nonlinear elimination method. Ann. Nucl. Energ. **114**, 301 (2018). https://doi.org/10.1016/j.anucene.2017.12.014
13. S. Hamilton, M. Berrill, K. Clarno et al., An assessment of coupling algorithms for nuclear reactor core physics simulations. J. Comput. Phys. **311**, 241–257 (2016). https://doi.org/10.1016/j.jcp.2016.02.012
14. D.A. Knoll, D.E. Keyes, Jacobian-free Newton-Krylov methods: a survey of approaches and applications. J. Comput. Phys. **193**, 357–397 (2004). https://doi.org/10.1016/j.jcp.2003.08.010

15. A. Peršič, T. Žagar, M. Ravnik et al., TRIGLAV: A program package for TRIGA reactor calculations. Nucl. Eng. Des. **318**, 24–34 (2017). https://doi.org/10.1016/j.nucengdes.2017.04.010
16. R. Henry, I. Tiselj, L. Snoj, Transient CFD/Monte-Carlo neutron transport coupling scheme for simulation of a control rod extraction in TRIGA reactor. Nucl. Eng. Des. **331**, 302–312 (2018). https://doi.org/10.1016/j.nucengdes.2018.03.015
17. M. Shayesteh, M. Shahriari, Calculation of time-dependent neutronic parameters using Monte Carlo method. Ann. Nucl. Energ. **37**(7), 901–909 (2009). https://doi.org/10.1016/j.anucene.2009.03.010
18. Y.G. Jo, B.H. Cho, N.Z. Cho, Nuclear reactor transient analysis by continuous-energy Monte Carlo calculation based on predictor-corrector quasi-static method. Nucl. Sci. Eng. **183**(2), 229–246 (2009). https://doi.org/10.13182/NSE15-100
19. S.H. Jang, H.J. Shim, Advances for the time-dependent Monte Carlo neutron transport analysis in McCARD. Nucl. Eng. Technol. **55**(7), 2712–2722 (2023). https://doi.org/10.1016/j.net.2023.04.007
20. T.E. Valentine, J.T. Mihalczo, MCNP-DSP: a neutron and gamma ray Monte Carlo calculation of source-driven noise-measured parameters. Ann. Nucl. Energ. **23**(16), 1271–1287 (1996). https://doi.org/10.1016/0306-4549(96)00004-7
21. A. Sun, Z. Chen, L. Kuang et al., Development and validation of the Monte Carlo code Magic for BNCT. Mod. Appl. Phys. **14**, 41 (2023). (in Chinese) https://doi.org/10.12061/j.issn.2095-6223.2023.040202
22. T.E. Booth, *A Weight (Charge) Conserving Importance-Weighted Comb for Monte Carlo, LA-UR-96-0051* (Los Alamos National Laboratory, NM (United States), 1996)
23. A. Ivanov, V. Sanchez, R. Stieglitz et al., High fidelity simulation of conventional and innovative LWR with the coupled Monte-Carlo thermal-hydraulic system MCNP-SUBCHANFLOW. Nucl. Eng. Des. **262**, 264–275 (2013). https://doi.org/10.1016/j.nucengdes.2013.05.008
24. L. Yu, W.L. Wang, C. Liu et al., Development and testing of a coupled SuperMC and SUBCHANFLOW code for LWR simulations. Ann. Nucl. Energ. **144**, 107465 (2020). https://doi.org/10.1016/j.anucene.2020.107465
25. R.M. Pearce, The Doppler effect in thermal reactors. J. Nucl. Energ. **13**(3–4), 150–175 (1961). https://doi.org/10.1016/0368-3265(61)90007-X
26. I. Uwe, S.V. Hugo, Validation of the subchannel code SUBCHANFLOW using the NUPEC PWR tests (PSBT). Sci. Technol. Nucl. Ins. **1**, 465059 (2012). https://doi.org/10.1155/2012/465059
27. K. Zhang, V.H. Sanchez-Espinoza, Coupling of TRACE and SubChanFlow based on the exterior communication interface. Prog. Nucl. Energ. **119**, 103040 (2020). https://doi.org/10.1016/j.pnucene.2019.103040
28. R. Henry, I. Tiselj, L. Snoj, CFD/Monte-Carlo neutron transport coupling scheme, application to TRIGA reactor. Ann. Nucl. Energ. **110**, 36–47 (2017). https://doi.org/10.1016/j.anucene.2017.06.018
29. M. García, D. Ferraro, V. Valtavirta et al., Serpent2-SUBCHANFLOW pin-by-pin modelling capabilities for VVER geometries. Ann. Nucl. Energ. **135**, 106955 (2020). https://doi.org/10.1016/j.anucene.2019.106955
30. M. Ravnik, R. Jeraj, Research reactor benchmarks. Nucl. Sci. Eng. **145**(1), 145–152 (2003). https://doi.org/10.13182/NSE03-A2370
31. I. Mele, M. Ravnik, A. Trkov, TRIGA MARK II benchmark experiment, Part I: Steady-state operation. Nucl. Technol. **105**(1), 37–51 (1994). https://doi.org/10.13182/NT94-A34909
32. I. Mele, M. Ravnik, A. Trkov, TRIGA Mark II benchmark experiment, Part II: pulse operation. Nucl. Technol. **105**(1), 52–58 (1994). https://doi.org/10.13182/NT94-1
33. A. Moorthi, A.K. Sharma, K. Velusamy, A review of sub-channel thermal hydraulic codes for nuclear reactor core and future directions. Nucl. Eng. Des. **332**, 329–344 (2018). https://doi.org/10.1016/j.nucengdes.2018.03.012
34. M.T. Simnad, The U ZrHx alloy: Its properties and use in TRIGA fuel. Nucl. Eng. Des. **64**, 329–344 (1981). https://doi.org/10.1016/0029-5493(81)90135-7
35. T. Matsumoto, N. Hayakawa, Benchmark analysis of TRIGA Mark II reactivity experiment using a continuous energy Monte Carlo code MCNP. J. Nucl. Sci. Technol. **37**(12), 1082–1087 (2000). https://doi.org/10.1080/18811248.2000.9714995
36. H.M. Dalle, C. Pereira, R.G. Souza, Neutronic calculation to the TRIGA Ipr-R1 reactor using the WIMSD4 and CITATION codes. Nucl. Eng. Des. **29**(8), 901–912 (2002). https://doi.org/10.1016/S0306-4549(01)00093-7
37. Z. Dong, J. Wu, X. Ma et al., Development and verification of a 281-group WIMS-D library based on ENDF/B-VII.1. Ann. Nucl. Energ. **91**, 189–194 (2016). https://doi.org/10.1016/j.anucene.2016.01.014